The Journal of Experimental Biology 210, 3538-3546
Published by The Company of Biologists 2007
doi:10.1242/jeb.009084

The acoustic mechanics of stick–slip friction in the California spiny lobster (*Panulirus interruptus*)

S. N. Patek*,† and J. E. Baio*

Department of Integrative Biology, University of California, Berkeley, CA 94720-3140, USA

*Both authors contributed equally to this work

†Author for correspondence (e-mail: patek@berkeley.edu)

Accepted 6 August 2007

Summary

The dynamic interplay between static and sliding friction is fundamental to many animal movements. One interesting example of stick–slip friction is found in the sound-producing apparatus of many spiny lobster species (Palinuridae). The acoustic movements of the spiny lobster's plectrum over the file are generated by stick–slip friction between the two surfaces. We examined the microscopic anatomy, kinematics, acoustics and frictional properties of the California spiny lobster (*Panulirus interruptus*) toward the goal of quantitatively characterizing the frictional and acoustic mechanics of this system. Using synchronous high-speed video and sound recordings, we tested whether plectrum kinematics are correlated with acoustic signal features and found that plectrum velocity is positively correlated with acoustic amplitude. To characterize the frictional mechanics of the system, we measured frictional forces during sound production using excised plectrums and files. Similar to rubber materials sliding against hard surfaces, the static coefficient of friction in this system was on average 1.7. The change in the coefficient of friction across each stick–slip cycle varied substantially with an average change of 1.1. Although driven at a constant speed, the plectrum slipped at velocities that were positively correlated with the normal force between the two surfaces. Studies of friction in biological systems have focused primarily on adhesion and movement, while studies of stick–slip acoustics have remained under the purview of musical acoustics and engineering design. The present study offers an integrative analysis of an unusual bioacoustic mechanism and contrasts its physical parameters with other biological and engineered systems.

Supplementary material available online at
http://jeb.biologists.org/cgi/content/full/210/20/3538/DC1

Key words: friction, coefficient, sliding, static, sound, bioacoustics, lobsters, Palinuridae, *Panulirus interruptus*, stick, slip, tribology.

Introduction

Stick–slip friction generates a vast array of oscillatory movements, ranging from earthquakes and squeaking doors to the tuned excitation of bowed stringed instruments (Benade, 1990; Persson, 2000; Rabinowicz, 1995). While the transitions between static and sliding friction are key to many biological movements (e.g. Goodwyn and Gorb, 2004; Niederegger and Gorb, 2006; Scherge and Gorb, 2001), biological sound production generated through periodic stick–slip frictional movements is both unusual and understudied. Here, we characterize the acoustic mechanics of stick–slip friction in the California spiny lobster (*Panulirus interruptus*) (Fig. 1) using a combination of kinematics, acoustic analyses and mechanical friction tests.

While virtually all translating surfaces experience friction forces that oppose movement and many surfaces simply slide relative to each other, stick–slip systems are defined by the presence of oscillations due to shifting magnitudes of friction and elastic energy storage between the two surfaces (Fig. 2). Most physics examples highlight the principles of friction in steady-sliding systems; a simple example is a block, which starts at rest and then reaches a constant velocity and constant frictional force as it slides down an inclined plane (Fig. 2A). In stick–slip systems, however, the relative movement of the two surfaces is cyclic, which results in a saw-toothed frictional force trace (Fig. 2B) (Persson, 2000). Stick–slip friction between two translating surfaces can cause a system to behave unpredictably (e.g. earthquakes and squeaky doors) or periodically (e.g. bowed-stringed instruments) (Fig. 2) (Persson, 2000; Urbakh et al., 2004). Understanding and controlling the dynamic behaviour of these systems have posed longstanding challenges to the fields of physics and engineering, and the result is a rich field of theoretical and applied research on the tribology of translating surfaces (Persson, 2000; Rabinowicz, 1995; Scherge and Gorb, 2001).

The only bioacoustic example of stick–slip friction described to date is found in the spiny lobsters (Fig. 1) (Patek, 2002; Patek, 2001; Patek and Oakley, 2003). Most spiny lobster species (Palinuridae) generate an anti-predator 'rasp' sound by rubbing the soft-tissue under-surface of the plectrum (an extension off of each antenna) over a cuticular, rectangular file below each eye (Fig. 1) (Lindberg, 1955; Meyer-Rochow and Penrose,

1974; Meyer-Rochow and Penrose, 1976; Moulton, 1957; Moulton, 1958; Mulligan and Fischer, 1977; Parker, 1878; Parker, 1883; Patek, 2002; Patek, 2001; Patek and Oakley, 2003; Phillips et al., 1980; Smale, 1974). The file's surface is covered with stiff, exoskeletal, microscopic shingles (approximately 10 μm width) and the plectrum consists of large, soft tissue ridges (approximately 0.1 mm in width) that are aligned parallel to their movement over the shingles. The shingle edges increase the frictional force between the two surfaces and oppose the movement of the plectrum as it sticks and slips posteriorly to generate pulsed sound.

Previous physiological experiments and a biomechanical model derived from bowed-stringed instruments demonstrated that spiny lobsters' pulsatile rasps are generated due to stick–slip friction, causing the plectrum to periodically slip then stick over the file surface (Fig. 1) (Patek, 2002; Patek, 2001). Similar to bowed-stringed instruments, such as the violin (Benade, 1990), the stick–slip mechanism in spiny lobsters can be modelled as a mass suspended between two springs (plectrum), which is excited when moved over a second, frictional surface (file) (Fig. 1). Supplementary material, Movie 1 and Movie 2, depict sound production and associated morphology, respectively.

The best-studied acoustic stick–slip system is found in bowed-stringed instruments. In these instruments, the bow cyclically sticks and slips over the string and generates vibrations that are coupled to the resonant body of the instrument (Benade, 1990). A player controls the oscillations of the string by varying the frictional forces between the bow and string. One way to do this is to simply increase the normal force by pressing the bow more firmly against the string, and as a result, increase the static friction force (Benade, 1990). In addition to the role of the human playing the violin, the material dynamics of the rosin applied to the bow hairs are responsible for the stick–slip behaviour of the bow rubbing over the string. Recent studies have shown that the rosin melts and hardens during each stick–slip cycle, suggesting a thermodynamic role in the stick–slip dynamics of this system (Day, 2007; Schumacher et al., 2005; Woodhouse et al., 2000).

In terms of biological systems, snail locomotion remains one of the few stick–slip examples that has been experimentally analyzed (Denny, 1980). Changes in the viscosity of the mucus lodged between the snail's foot and substrate enable snails to periodically oscillate between static and kinetic friction (Denny, 1980; Mahadevan et al., 2004). During locomotion, translational waves travel down the foot of a snail. The leading edge of the wave stresses the mucus and induces the liquid phase (kinetic friction). Just behind this edge, the mucus solidifies and resists the movement of the foot, thereby creating enough static friction for the foot to push against and for the snail to move forward.

Both biological and engineered frictional systems are most commonly described in terms of the coefficient of friction (μ), which is a dimensionless number that expresses the relative contribution of the frictional force opposing movement (F_f) to the normal force (F_n) between two contacting surfaces:

$$\mu = F_f / F_n . \quad (1)$$

For the purposes of this paper, μ refers generally to the coefficient of friction as a function of time (t) [i.e. $\mu(t)$]. The static friction coefficient (μ_s) occurs at the time point when movement begins (Heslot et al., 1994). The coefficient of kinetic friction (μ_k) is measured during sliding. However, μ_k is difficult to measure in stick–slip systems, because the sliding phase of stick–slip systems occurs over a changing velocity and, often, a very short time period (Heslot et al., 1994). Some argue that it is not possible to measure μ_k in stick–slip systems, because of the changing velocity (Gratton and Defrancesco, 2006); others examine μ_k as a function of time and surface–surface interactions (Heslot et al., 1994). For example, Heslot et al. determined that μ_k is proportional to the natural logarithm of the constant driving velocity of one of the surfaces (Heslot et al., 1994).

The magnitude of the change in μ and the maintenance of a periodic stick–slip motion are caused by an interdependent constellation of factors, including velocity, elastic energy storage and normal force (Heslot et al., 1994; Persson, 2000; Urbakh et al., 2004; Woodhouse et al., 2000). These parameters can be used to characterize the rapid transitions between static and sliding friction and, in order to model the system, calculate spring constants and approximate surface dynamics (Scherge and Gorb, 2001; Yoshizawa and Israelachvili, 1993). Most stick–slip systems have a bounded region in which periodic stick–slip movements occur given a particular range of driving velocities and loads (Day, 2007; Persson, 2000). By measuring

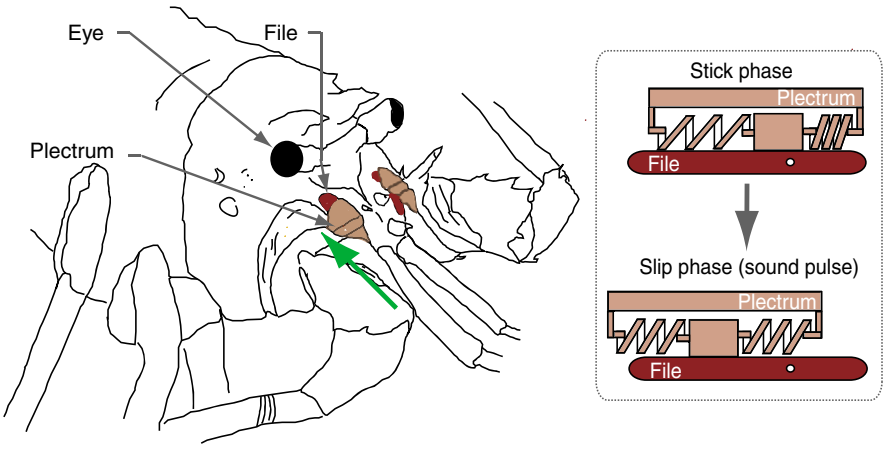

Fig. 1. The sound-producing morphology of the California spiny lobster (*Panulirus interruptus*). A pair of plectrums (pink), an extension off each antenna, rub posteriorly over the files (dark red) to produce sound. The green arrow indicates the direction of the plectrum's movement when producing sound. Inset: a mass-and-spring representation of the acoustic stick–slip mechanism found in spiny lobsters (Patek, 2002; Patek, 2001). The plectrum (pink) is modeled as a moveable component with a mass sandwiched between two springs. The plectrum moves across the file (dark red), which is fixed in place. Each time the plectrum slips, a pulse of sound is produced. Movie 1 and Movie 2 in supplementary material show sound production and associated morphology, respectively.

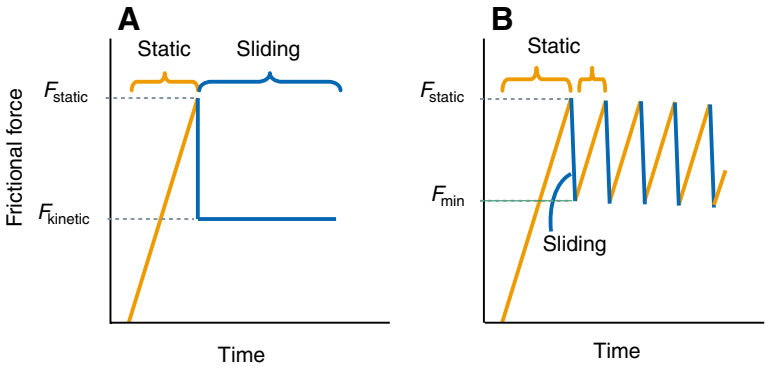

Fig. 2. Sliding friction dynamics in steady sliding (A) and periodic stick–slip motion (B). During the static phase (orange), frictional forces increase linearly until they reach the critical frictional force value (F_{static}) when the slip phase (blue) starts. (A) In steady sliding systems, the kinetic friction force ($F_{kinetic}$) is measured once the system reaches a constant sliding velocity. (B) In stick–slip motion, however, the slip phase is immediately followed by another stick phase. Thus, stick–slip systems often never reach a constant velocity during the slip phase, thereby making calculations of $F_{kinetic}$ difficult. In the present study, we calculated the maximum change in the coefficient of friction (μ) per stick–slip cycle by using the time points at which maximum and minimum frictional forces occurred during each stick–slip cycle, which correspond to F_{static} and the minimum frictional force (F_{min}), respectively. (Adapted from Persson, 2000.)

the coefficients of friction across a range of loads and velocities, it is possible to define the mechanical space within which periodic stick–slip motion occurs. While the existing mechanical model of the acoustic mechanism in spiny lobsters provides a heuristic explanation of the system, these underlying physical parameters governing the periodic stick–slip behaviour have yet to be measured.

The primary goal of this study was to quantitatively characterize the acoustic mechanics of stick–slip sound production in the California spiny lobster (*P. interruptus*). The first step in understanding a frictional mechanism is to measure the frictional forces, the relative movement of the surfaces, and the functional consequences of variation in these parameters. Thus, in the spiny lobster system, we examined the kinematics, friction and acoustics in live animals and excised sound-producing structures. First, we examined the microscopic anatomy of the plectrum and file surfaces that had not previously been described in this species. Second, we synchronously recorded the sounds and movement of live, sound-producing animals to test whether plectrum kinematics are correlated with the acoustics of the rasp. Third, we measured the coefficients of friction and frictional forces in isolated plectrum and file preparations with which we characterized the stick–slip frictional mechanism in spiny lobsters. Ultimately, these results can be used to model variation in acoustics and friction mechanics within and across palinurid species, to understand the evolution of biological friction systems, and to contribute to the fascinating and complex realm of stick–slip mechanics in both engineered and biological systems.

Materials and methods

Microscopic anatomy of the file and plectrum

The plectrums and files of five *Panulirus interruptus* Randall 1842 (Crustacea: Decapoda: Palinuridae) individuals (85–90 mm carapace length, Catalina Offshore Products, San Diego, CA, USA) were prepared and analyzed using environmental scanning electron microscopy (ESEM). Specimens were fixed in 2% glutaraldehyde (0.1 mol l^{-1} sodium cacodylate buffer), rinsed three times for 15 min (0.1 mol l^{-1} sodium cacodylate buffer), then soaked in 1% osmium tetroxide (0.1 mol l^{-1} sodium cacodylate buffer, pH 7.2). After 2 h, the specimens were again rinsed three times for 5 min using 0.1 mol l^{-1} sodium cacodylate buffer. Dehydration was achieved through a series of ethanol solutions gradually increasing from 35% to 100% ethanol. After dehydration, specimens were critical-point-dried (Tousimis AutoSamdri 815, Series A, Critical Point Drier, Rockville, MD, USA), mounted on stubs using carbon dots, and then coated to 20 nm with palladium alloy (BIO-RAD E5400 Sputter Coater, Hercules, CA, USA). Once prepared, specimens were rendered at 20.0 kV (Philips XL-30 Scanning Electron Microscope).

We measured the medial–lateral and anterior–posterior dimensions of 30 shingles at five locations along the length of each file. The length and width of five plectrum ridges in four specimens also were measured. With the shingle dimensions and the kinematics of the plectrum movements (described below), we calculated the rate of shingle excitation (shingles s^{-1}) given the speed of the plectrum over the file.

Rasp kinematics and acoustics

Five California spiny lobsters *Panulirus interruptus* were purchased from commercial sources (85–88 mm carapace length, Catalina Offshore Products) and used for the kinematic and acoustic experiments. We measured 5–6 rasps per individual. Each rasp consists of a series of pulses, thus we measured a total of 18–28 pulses per individual. Animals were housed in 395 l and 710 l tanks with filtered recirculating, synthetic seawater (17–19°C). Shrimp and mussels were provided 5 days per week.

Acoustic and kinematic data were simultaneously recorded using high-speed images (3000 frames s^{-1}, 0.33 ms shutter duration, 1024×1024 pixel resolution, APX-RS high speed video camera, Photron USA Inc., San Diego, CA, USA) and sound (0.1 Hz–80 kHz, –206.1±0.25 dB re 1V/μPa, Model 8104 hydrophone, Brüel and Kjaer, Nærum, Denmark; 1 Hz–1 MHz, VP2000 voltage preamplifier, Reson, Slangerup, Denmark). The acoustic data were sampled at 30 000 samples s^{-1} (preamplifier set as bandpass filter: 1 Hz–15 kHz) using an analog-to-digital converter coupled to the high-speed video camera (Multi-Channel Data Link; Photron USA Inc.).

In order to track the movements of the plectrum over the file and correct for off-axis positioning of the lobster relative to the camera's plane of view, reflective dots were attached to the plectrum and antennular plate. The centroids of these reflective dots were tracked using a custom, automated, digital image

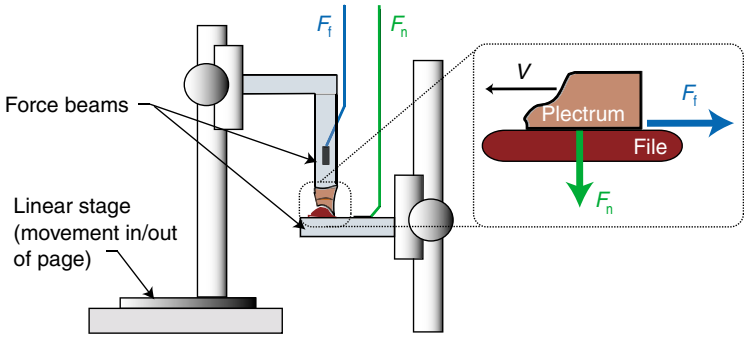

Fig. 3. A schematic of the device used for measuring frictional forces between the file (dark red) and plectrum (pink). The plectrum was mounted on a linear stage, which moved the plectrum over the file at velocity (V) (directed into/out of the page). A force beam was mounted on the vertical beam to measure the frictional force, F_f, which is directed opposite to the movement of the plectrum. A second force beam was mounted on a manual translation stage with which the normal force (F_n), applied orthogonally between the two surfaces, could be varied. The inset shows the directions of the force vectors; note that this drawing is rotated 90° relative to the apparatus diagram.

analysis program (v.2006b, Matlab, The Mathworks, Natick, MA, USA). One dot was attached to the plectrum while the other two were affixed, at a known distance apart, to the side of the file and parallel to the movement of the plectrum. This second pair of dots was used to correct for off-axis positioning of the lobster during sound production. Changes in this distance during a video sequence provided the angle between the plane of the camera and the movement of the plectrum. Absolute scaling was determined by placing a ruler perpendicular to the camera at the focal distance of the lobster during recording. The ruler provided a pixel:distance conversion perpendicular to the camera's plane of view with which the actual distance between the two calibration dots on the lobster was calculated. The distance traveled by the reflective dot on the plectrum was tracked throughout each sequence.

In addition to tracking the displacement of the plectrum over the file, the durations of slip movements, peak velocity and average velocity of the plectrum were determined. The velocity profile of the plectrum movement was calculated by taking the derivative of the displacement data. In order to reduce noise and accurately measure the peak velocities, the displacement data were first interpolated and then filtered with a 700 Hz low-pass filter (5th order Butterworth filter; v2006b, Matlab). Average velocities were calculated by taking the root mean square (RMS) of each velocity profile.

We measured the timing and amplitude of each rasp associated with the plectrum measurements described above. The acoustic data were first filtered with a 60 Hz high-pass filter, then the onset and offset times of each pulse within a rasp were measured. In addition, the peak voltage and RMS amplitude of each acoustic pulse were measured.

We examined the correlation between plectrum movement and sound production, specifically in terms of the onset/offset of sound production, pulse duration, pulse frequency, plectrum slip distance, plectrum velocity and pulse amplitude. Because the position of the hydrophone relative to the lobster's sound-producing apparatus varied across recording sequences, we scaled the peak amplitude of sound production within each sequence to a value of 1, such that pulses were measured as a fraction or multiple of the reference value. While the onset of each pulse was clear in the acoustic data, the offset was often obscured by acoustic reverberations in the recording tank. Thus, we predicted that the acoustic measurements of pulse duration would be greater than the kinematic measurements of slip duration.

The statistical correlation between plectrum movement and sound amplitude was analyzed using a nested least-squares model with rasps identified as random effects (repeated-measures design using the Residual Maximum Likelihood method) (JMP v. 5.0.1). Because the hydrophone was not held at a constant distance from the animals across experiments, the statistical analyses incorporated the raw amplitude data as well as amplitude data in which the pulses within each rasp were scaled to a reference value (as above).

Stick–slip friction measurements

To determine the coefficient of friction, we built a friction-measurement device to record the frictional (F_f) and normal (F_n) forces between the plectrum and file surfaces as they generated sound (Fig. 3). Friction measurements were recorded in nine plectrums and files from nine individuals (82.5–90.2 mm carapace length; Catalina Offshore Products). Ten experiments were conducted on each plectrum/file unit.

An excised plectrum and file were mounted on separate force beams positioned perpendicularly to each other (TBS-10 lb sensors, Transducer Techniques, Temecula, CA, USA). The plectrum was glued (Instant Krazy Glue, Columbus, OH, USA) to the vertical beam attached to a linear translation stage (0.5 μm resolution, ILS50CC translation stage, ESP300 universal motion controller/driver, Newport, Irvine, CA, USA). The vertical beam was positioned orthogonally to the stage and thus measured the frictional force opposing the movement of the plectrum. The file was glued to the horizontal beam located at the side of the translation stage. The horizontal beam measured the normal force that was applied perpendicularly to the movement of the plectrum. Both beams were calibrated by applying a range of known forces, measuring the corresponding voltage response, and constructing a linear interpolation with which voltages (V) were converted to Newtons (N).

Kinematic and force data were collected simultaneously as the translation stage moved the plectrum over the file. Force data were obtained *via* a custom data acquisition program (v.2006b, Matlab) through an analog-to-digital computer board (50 kHz sample rate, PCI-MIO-16E-4 DAQ board, National Instruments, Austin, TX, USA). The normal force between the plectrum and file was adjusted using a rod positioning system (Newport, Irvine, CA, USA) attached to the file and horizontal force beam (Fig. 3). Experiments were conducted across a range of normal forces (0.5–5 N) that produced a typical rasp sound.

The translation stage operated at a constant velocity (100 mm s^{-1}) and step size (5 mm), which drove the plectrum's intermittent, stick–slip movement. Before each experiment, the

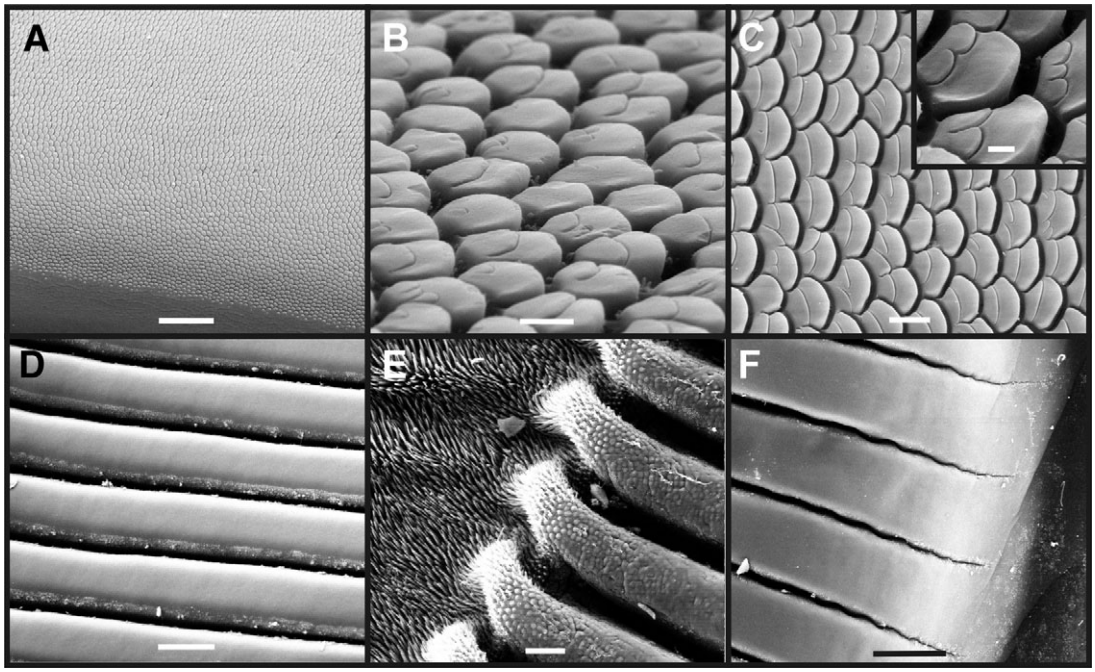

Fig. 4. Scanning electron micrographs of the file and plectrum surfaces. Anterior is to the right of the page in all images. (A) The dorsal file surface is covered with microscopic shingles with their leading edges oriented anteriorly. A groove on the medial edge of the file (medial to bottom of page) guides a knob on the plectrum such that the plectrum slides anteriorly and posteriorly in a controlled alignment, similar to a sliding door in its track. Scale bar, 100 μm. (B) An oblique view of the file shingles shows the distinct separation of the shingles and the additional ridge running medio-laterally on most shingles. Scale bar, 5 μm. (C) A dorsal view of file shingles (scale bar, 10 μm; inset, 2 μm) shows the more prominent frictional edges of the shingles on the anterior side, analogous to shingles on the roof of a house. (D) The ventral surface of the plectrum is composed of soft-tissue plectrum ridges that run parallel to their antero-posterior movement over the file. Scale bar, 100 μm. (E) The leading edges (posterior) of the plectrum ridges fuse with the setae on the ventral surface of the plectrum. Scale bar, 50 μm. (F) The anterior edge of the hemisphere of plectrum ridges ultimately attaches to the ventral cuticle of the antennal base. Scale bar, 100 μm.

plectrum and file surfaces were saturated with artificial seawater. In addition, the plectrum knob was positioned in the groove on the file (Fig. 4) such that the alignment was similar to the lobster's natural movement. We tracked the plectrum's movement by attaching a reflective dot, filming the movement (3000 frames s^{-1}, 0.33 ms shutter duration, 1024×1024 pixel resolution, Photron APX-RS high speed video camera; Photron Inc.), and using the automated point-tracking system described in the previous section. We compared these plectrum movements to the kinematics measured in live individuals (described in previous section). The plectrum displacements were used to determine the times at which the plectrum started to slip as it was forced over the file. Slip durations and slip periodicities also were measured.

The coefficient of friction was calculated by dividing the filtered friction results by the filtered normal force results, yielding values of μ as a function of time [$\mu=\mu(t)$ (see Eqn 1)]. A low-pass filter at the resonant frequency of the force beams, 280 Hz, was applied to the force traces. Typically, the initial stages of stick–slip cycles are chaotic and then transition to more uniform oscillations. We also observed this phenomenon in the experimental rasps; thus, in our analysis, we only included the three stick–slip cycles at the most uniform portion of each rasp.

The peak static coefficient (μ_s) was defined as the time point along the curve $\mu(t)$ when the plectrum started to move (Fig. 2). As mentioned earlier, it is difficult to measure the sliding coefficient of friction, because the velocity changes throughout the slip period and, in our case, the beam reverberations obscured the transition between the slip and stick phases (see Results). Instead, we calculated the maximum change in $\mu(t)$ for each stick–slip cycle examined. This value represents the maximum difference between the static and sliding coefficients of friction. The force traces of the static phase were fit with a least-squares linear curve and changes in μ were determined by calculating the differences of the values of the line fits at times just before and after the slip phase. Due to force beam resonances, it was necessary to interpolate the values of μ from these curve fits.

The peak slip velocity and average load during the slip phase also were determined for each stick–slip cycle. The velocity profile of the plectrum movement was calculated by taking the derivative of the displacement data. In order to reduce noise and accurately measure the peak velocities, the displacement data were filtered with a 700 Hz low-pass filter (5th order Butterworth filter; v.2006b, Matlab). Average normal forces were calculated by taking the RMS of the load profile during the slip phase. The durations of the stick–slip cycles were determined from the kinematic displacement data.

The statistical relationships between the changes in the frictional coefficient, slip velocity and slip frequency were analyzed using a general linear model (analysis of covariance, ANCOVA) to examine the relationships between these

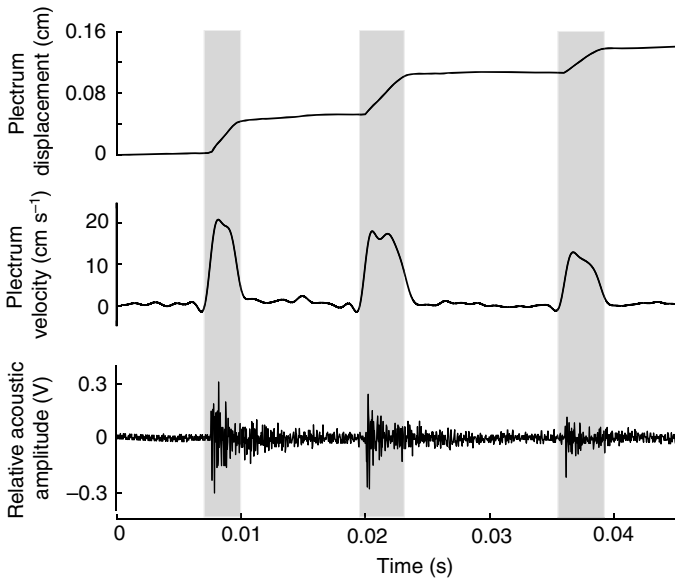

Fig. 5. Synchronous measurements of plectrum kinematics and acoustic signals. Grey regions indicate the slip phases of the stick–slip cycling. A pulse of sound is produced each time the plectrum slips over the file.

variables and the effects of individual, trial and individual by trial on the resulting correlations (JMP v. 5.0.1).

Descriptive statistics are reported as the mean value ± one standard deviation (s.d.) from the mean.

Results

Microscopic anatomy of the file and plectrum

Files from *P. interruptus* were covered with microscopic shingles and the plectrums consisted of soft-tissue ridges that extended parallel to their movement over the file (Fig. 4). The average medial/lateral width of the shingles was 12.3±0.9 μm and the mean anterior/posterior length was 7.4±0.7 μm. There were significant effects of individual and shingle location on measurements of shingle width (nested ANOVA, F=24.565, P<0.0001) and shingle length (nested ANOVA, F=6.952, P<0.0001). The plectrum ridges were on average 0.11±0.01 mm in width and 2.25±0.04 mm in length. Individuals were not significantly different in ridge width (one-way ANOVA, F=0.1565, P=0.9) nor ridge length (one-way ANOVA, F=1.661, P=0.2). The spacing between the ridges ranged from a nearly continuous surface at the anterior limit (Fig. 4F) to an average 38±8 μm at the posterior limit (Fig. 4E) (one-way ANOVA, F=0.0954, P=0.96). At the posterior limit of the plectrum ridges, the ridges gradually merged with a dense matt of setae (Fig. 4E). The ridges in this posterior region appeared to be made of fused setae.

The width of each plectrum ridge spanned approximately ten shingles, and the length of the ridges spanned hundreds of shingles. Thus, as a plectrum slips over the file, it articulates with thousands of shingles rather than exciting a single region or series of shingles.

Rasp kinematics and acoustics

The correspondence between the kinematic and acoustic measurements of each rasp was analyzed by comparing pulse duration to slip duration, acoustic amplitude to plectrum speed, and pulse rate to plectrum speed. The number of pulses measured was identical in high-speed video and hydrophone recordings and consisted of an average 4.5±0.9 pulses (range 3–7). Consistent with the expected acoustic reverberations in the tank compared to the discrete offset captured by kinematic measurements, the mean acoustic measurement of pulse duration was 7.9±2.0 ms (range 1.4–19.9) whereas the mean kinematic measurement of slip duration was 3.6±1.3 ms (range 0.6–9.0) (Fig. 5). Similarly, the acoustic pulses s^{-1} (mean 87.6±15.9; range 55.4–136.7) were lower than the kinematic pulses s^{-1} (mean 94.9±14.7; range 61.6–133.5).

Plectrum speed and acoustic amplitude were positively correlated. During each slip, the plectrum moved an average 3.8±1.0 mm (range 0.22–10.8) at an average speed of 11.3±3.1 cm s^{-1} (range 2.3–29.6) and average peak speed of 22.8±3.7 cm s^{-1} (range 7.0–41.3). Plectrum speed was positively correlated with pulse amplitude, whereas plectrum slip distance was not (Table 1). Peak plectrum speed was strongly positively correlated with all measures of pulse amplitude and average plectrum speed was positively correlated with RMS average pulse amplitude (Table 1). None of the amplitude measures were correlated with plectrum slip displacement.

Pulse rate increased with plectrum speed. Both peak and mean speeds were positively correlated with the kinematic measurement of pulse rate (mean speed: R^2=0.5511, P=0.004, significant individual effects, P=0.002; peak speed: R^2=0.4132,

Table 1. *Statistical analyses of the effect of plectrum kinematics on sound amplitude*

	Peak pulse amplitude (V)			RMS pulse amplitude (V)			Scaled peak pulse amplitude			Scaled RMS pulse amplitude		
	R^2	F-ratio	P-value	R^2	F-ratio	P-value	R^2	F-ratio	P-value	R^2	F-ratio	P-value
Plectrum speed (cm s^{-1})												
Peak	0.84	15.9	0.0001*	0.80	16.0	0.0001*	0.25	16.0	0.0001	0.43	36.1	<0.0001
Average	0.82	3.6	0.06	0.77	5.7	0.02				0.29	12.3	0.0007
Plectrum slip distance (cm)	0.81	0.04	0.8	0.75	0.2	0.6				0.16	0.7	0.4

Asterisks indicate significant differences across individuals in two of the tests. Two results are not shown, because they violated statistical assumptions of the repeated-measures tests (negative-tending variances).

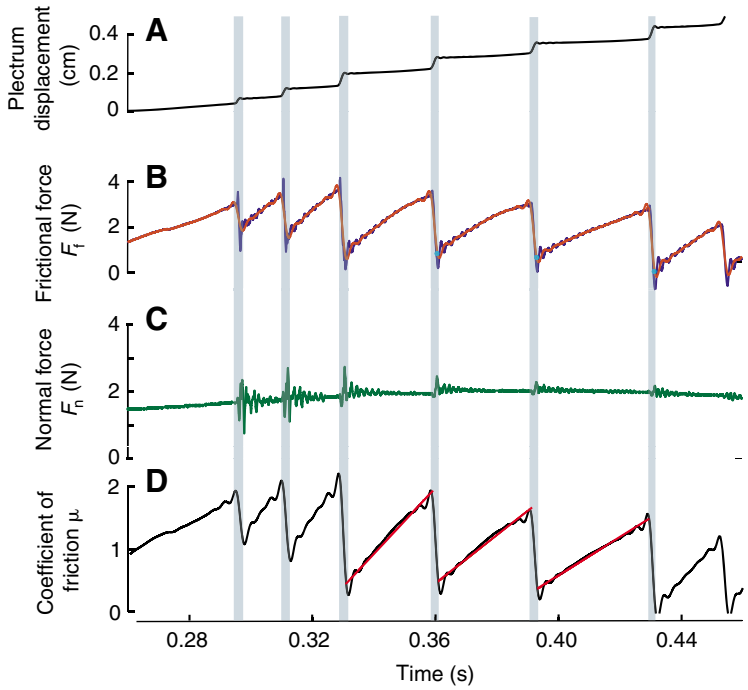

Fig. 6. Synchronous measurements of plectrum displacement (A) frictional forces (B, F_f; C, F_n) and coefficient of friction (D, μ). The oscillating force and coefficient of friction waveforms are a product of the stick–slip friction dynamics of the plectrum moving over the file. Each force trace (F_f and F_n) is correlated with the movement of the plectrum. In B, the raw data are depicted in blue and the filtered data (low pass filter at 280 Hz) in red. Grey regions label the slip phases of the stick–slip cycling. In D (coefficient of friction), the linear fits of the static friction regions of the waveform are depicted in red.

P=0.04, non-significant individual effects, P=0.07). Acoustic measurements of pulse rate were not significantly positively correlated with plectrum speed (P>0.05).

Given the average plectrum velocity and shingle dimensions, shingles were excited at approximately 1530 shingles s^{-1}, which was distinct from the average acoustic pulse rate of 90 pulses s^{-1}.

Stick–slip friction measurements

The static coefficient of friction (μ_s) ranged from 0.4–3.5 (mean 1.7±0.3). As predicted by the stick–slip model (Fig. 2), the coefficient of friction decreased rapidly when the plectrum started to move (Fig. 6). The maximum changes in μ over the course of each stick–slip cycle were on average 1.1±0.3 and ranged from 0.1–3.6.

Slip velocity, stick–slip frequency (equal to acoustic pulse rate), μ_s and change in μ varied as we applied a range of normal forces from 0.5–5 N. Although the stage was driven at a constant velocity (10 cm s^{-1}), the plectrum slipped at velocities ranging from 7.6–75.7 cm s^{-1} (mean: 28.0±7.7 cm s^{-1}). Plectrum velocity was significantly positively correlated with F_n in six out of the nine individuals, but tests for individual effects on the overall dataset were significant (whole model: R^2=0.6058; F=14.01, P<0.0001; significant effects of F_n, individual, and individual by trial). The change in μ was positively correlated with velocity, again with significant effects of dataset and trial by dataset (whole model: R^2=0.8729, F=29.99, P<0.0001) while μ_s was not correlated with velocity (whole model: R^2=0.8653, F=56.03, P<0.0001; no significant effect of velocity; significant effects of dataset, trial and trial by dataset). The stick–slip cycle frequency was negatively correlated with change in μ (R^2=0.3323, F=8.82, P<0.0001; significant effect of dataset) and with F_n (R^2=0.4054, F=12.58, P<0.0001; significant effect of dataset). Peak plectrum velocity and stick–slip cycle frequency were negatively correlated (R^2=0.7209; F=22.39, P<0.0001; significant effect of dataset).

Discussion

Through the integration of acoustics, kinematics, functional morphology and friction mechanics, we present the first mechanical characterization of a bioacoustic stick–slip mechanism. We found that *P. interruptus* has similar morphological and acoustic features to previously studied spiny lobsters, with soft tissue plectrum ridges that articulate against the frictional edges of cuticular shingles to produce pulsed stick–slip sounds. The kinematic analyses suggested that plectrum movements influence signal characteristics, while the friction results provided a mechanical explanation for the variation in plectrum kinematics and acoustics. Plectrum velocity and the normal force between the plectrum and file played important roles in the acoustic and frictional properties of this system. This study provides the essential framework for future stick–slip models, not only for engineering design, but also for understanding the individual control of sound production and, ultimately, explaining the evolutionary implications of varying stick–slip frictional properties across spiny lobsters.

California spiny lobsters shared the general acoustic and morphological features as reported in other palinurids (*Panulirus argus*, *Palinurus elephas* and *Panulirus longipes*) (Fig. 4) (Meyer-Rochow and Penrose, 1974; Meyer-Rochow and Penrose, 1976; Patek, 2002; Patek and Oakley, 2003; Phillips et al., 1980; Smale, 1974). The medial–lateral ridges present on each shingle in *P. interruptus* were similar to other *Panulirus* species (Meyer-Rochow and Penrose, 1976; Moulton, 1957; Moulton, 1958; Patek, 2002), although they are not present in *Palinurus* (Patek, 2002) or *Puerulus* species (S.N.P., personal observations). These surface asperities are likely to increase the friction between the plectrum and file surfaces compared to the smooth shingle surfaces of other palinurids. The plectrum ridges appeared to be derived from setae, given that the posterior limits of the plectrum ridges were constructed of fused setal bases (Fig. 4E). The acoustic signal features of *P. interruptus* were in the range of other spiny lobsters (Patek and Oakley, 2003) with short duration pulses (7.9 ms) and moderate pulse rates (90 pulses s^{-1}).

Given the basic principles of stick–slip friction, can lobsters behaviourally control acoustic signal features and does variation in shingle anatomy across species lead to differences in stick–slip acoustics? One possible avenue for control of the system is through plectrum velocity and normal force. The

plectrum is moved over the file *via* a tonic contraction of the promoter muscle, which extends from the base of the antennae to the dorsal cephalothorax (Patek, 2002; Paterson, 1968). A series of depressor muscles rotate the antennae ventrally and a lateral levator muscle attaches to the lateral edge of the antennae and extends to the ventral surface of the cephalothorax (Patek, 2002; Paterson, 1968). In addition to the promoter muscle, the lateral levator muscle is often activated during sound production (Patek, 2002; Paterson, 1968). Thus, variation in plectrum velocity and normal force is likely to be mediated by the promoter and lateral levator muscles. In particular, the promoter muscle has two lobes, which cover a substantial area of the dorsal and lateral cephalothorax. Differential activation of these lobes may vary plectrum velocity and load.

Plectrum velocity varied substantially in both the analyses of sound production in live animals and in the friction experiments. Together, these two sets of experiments shed light on the relevance to sound production and mechanical causes of this variability. Although the constant stage velocity (10 cm s^{-1}) matched the average plectrum velocity (11 cm s^{-1}) in live animals, the variation in velocity in both systems was fairly extreme, ranging from 7 to 76 cm s^{-1}. The fact that the stage velocity was held constant, yet the plectrum still slipped at such a wide range of velocities, suggests that the variation in plectrum velocity and correlated acoustic amplitude observed in live animals may not be under direct control by rates of muscle contraction and may instead be a product of the stochasticity of oscillating stick–slip systems.

An alternative explanation for the correlation between plectrum velocity and acoustic amplitude in live animals is suggested by the positive correlation of plectrum velocity and normal force in the friction experiments. This correlation implies that if pulse amplitude is controlled by muscle contractions, and is not a stochastic effect of the mechanism, increasing the normal force between the plectrum and file may increase the acoustic amplitude. Changes in the relative contraction amplitude of the lateral levator or the lateral and medial lobes of the promoter muscle may alter the normal force between the plectrum and file.

The rate of stick–slip cycling (equivalent to the acoustic pulse rate) typically is attributed to the velocity of the driving surface (Persson, 2000; Scherge and Gorb, 2001). A minimum velocity is required to establish a stick–slip behaviour and characteristic frequency; after a maximum velocity is reached, the system again ceases to operate in the stick–slip realm. Between these two critical velocities, the stick–slip frequency typically increases with velocity (Scherge and Gorb, 2001). We did not investigate the velocity limits between which stick–slip occurs in this system, focusing instead on the approximate range utilized by the lobster. However, within this range in our experiments, the relationship between velocity and stick–slip frequency was inconclusive, if not contradictory, between the live animal and friction experiments. In future studies, it would be informative to expand the range of stage velocities to explore this 'space' of stick–slip behaviour and to determine the extent to which lobsters can vary the acoustic pulse rate of their signals by changing the plectrum velocity or normal force.

The other major avenue for varying acoustic signal features and stick–slip behaviour is through the structural, frictional interactions of the plectrum and file surfaces. The average μ_s of *P. interruptus* was 1.7, which is in the same range as an elastomeric material (e.g. rubber) interacting with a hard metallic surface (1.0–4.0) (Ashby and Jones, 1996). Although we were unable to accurately measure μ_k because of the beam resonances and changing velocity of the two surfaces throughout the slip phase, we were able to characterize relative changes in μ (Fig. 6). The maximum change in μ averaged 1.1 and spanned a 30-fold range in values. Thus, while the stick–slip cycling maintained a characteristic form across the experiments (Figs 2, 6), the magnitude of the transitions varied substantially.

Parallels between the friction dynamics of ant adhesive foot pads also have been drawn with the friction behaviour of engineered rubber materials (Federle et al., 2004); in the ant system, μ_s was estimated at 2.2. Similar to the spiny lobsters, a liquid layer was present in this frictional system; however, based on their μ_s estimates, the surface asperities exceeded the height of the liquid layer, such that the surface dynamics were determined by the rubbery behaviour of the ant's foot pad rather than fluid dynamics. In contrast, the dry frictional system of a heteropteran wing-locking mechanism has an average μ_k of 0.1–0.2 when slid at a maximum velocity of 18.6 cm s^{-1}, to which the authors draw a comparison with 'Babbitt alloy sliding over steel' (Goodwyn and Gorb, 2004).

The presence of saltwater in the spiny lobster system almost certainly influences the surface dynamics and friction forces. Static friction between elastic rubber balls and a smooth glass plate is correlated with the viscosity of the films of water (thickness >10 nm) sandwiched between the two surfaces (Roberts, 1971; Roberts and Tabor, 1971). Previous investigations have noted that rubber materials warp and conform to the interacting surface (Ashby and Jones, 1996). This conforming process increases the overall contact area between the two surfaces, which can either supersede the effects of a fluid layer or simply add an additional variable to the surface dynamics (Federle et al., 2004). Our experiments were conducted in air, because of the considerable challenges of constructing the friction measurement system for immersion in saltwater. Although we took great care to saturate the surfaces with saltwater, it is possible that the absence of the surrounding body of water affected our friction measurements.

The soft, elastic tissue of the plectrum (Figs 1, 4) is likely to be the primary site of elastic energy storage in this system. Release of stored elastic energy occurs during the slip phase; it is also during this time that sound is generated. Controlled engineering experiments of stick–slip dynamics have shown that most of the stored energy is dissipated during the slip phase, with a relatively small proportion released due to momentum transfer when the surface sticks (Klein, 2007). The spring constant of the materials in stick–slip systems is central to their behaviour (Heslot et al., 1994; Klein, 2007), thus it would be informative to examine the material and mechanical properties of the plectrum ridges.

Whether the stick–slip system in spiny lobsters can be attributed to surface asperities, fluid dynamics at the surface interface, or emergent dynamics of the elastic plectrum and stiff file materials (e.g. Mahadevan et al., 2004) is not yet known. The relative roles of friction and mechanical interlocking

between the file's shingles and plectrum surface should be evaluated. While the scale of each slip by the plectrum (average 3.8 mm) far exceeds the scale of the shingles (average 7.4 μm), it is possible that the mechanical connections between the plectrum and shingles play an important role in mediating the overall stick–slip behaviour of the system. Further investigation of the microscopic asperities, material properties and surface interactions is needed in order to fully characterize the influence of both the surface roughness of the file and the fluid dynamics of the film of saltwater between the plectrum and file.

Understanding and characterizing the dynamics of friction have presented longstanding challenges to engineers, musicians and biologists. The spiny lobster's use of stick–slip friction to generate acoustic signals offers an interesting example of a complex, stochastic, yet robust, biological system. Through the integration of physics, engineering and acoustics, new insights into the evolutionary history and mechanics of biological friction systems will continue to emerge.

Special thanks to S. Serafin for inspiring this study. We thank S. Gorb, M. deVries, S. Sane, A. Spence and the UC Berkeley Biomechanics seminar for their helpful comments and advice. N. Valencia, L. Shipp, M. deVries and R. Tigue assisted with experiments. Funding was provided by a UC Berkeley Committee on Research Junior Faculty Research Grant (S.N.P.).

References

Ashby, M. F. and Jones, D. R. F. (1996). *Engineering Materials 1, An Introduction to their Properties and Applications*. Oxford: Butterworth-Heinemann.

Benade, A. H. (1990). *Fundamentals of Musical Acoustics*. New York: Dover Publications.

Day, L. (2007). Analyzing the tribology of sound. *Tribol. Lubric. Technol.* **63**, 28-39.

Denny, M. (1980). The role of gastropod pedal mucus in locomotion. *Nature* **285**, 160-161.

Federle, W., Baumgartner, W. and Hölldobler, B. (2004). Biomechanics of ant adhesive pads: frictional forces are rate- and temperature-dependent. *J. Exp. Biol.* **206**, 67-74.

Goodwyn, P. J. P. and Gorb, S. N. (2004). Frictional properties of contacting surfaces in the hemlytra hindwing locking mechanism in the bug *Coreus marginatus* (Heteroptera, Coreidae). *J. Comp. Physiol. A* **190**, 575-580.

Gratton, L. M. and Defrancesco, S. (2006). A simple measurement of the sliding friction coefficient. *Phys. Educ.* **41**, 232-235.

Heslot, F., Baumberger, T., Perrin, B., Caroli, B. and Caroli, C. (1994). Creep, stick–slip, and dry-friction dynamics – experiments and a heuristic model. *Phys. Rev. E* **49**, 4973-4988.

Klein, J. (2007). Frictional dissipation in stick–slip sliding. *Phys. Rev. Lett.* **98**, 1-4.

Lindberg, R. G. (1955). Growth, population dynamics, and field behavior in the spiny lobster, *Panulirus interruptus* (Randall). *Univ. Calif. Publ. Zool.* **59**, 157-248.

Mahadevan, L., Daniel, S. and Chaudhury, M. K. (2004). Biomimetic ratcheting motion of a soft, slender, sessile gel. *Proc. Natl. Acad. Sci. USA* **101**, 23-26.

Meyer-Rochow, V. B. and Penrose, J. D. (1974). Sound production and sound emission apparatus in puerulus and postpuerulus of the western rock lobster. *J. Exp. Zool.* **189**, 283-289.

Meyer-Rochow, V. B. and Penrose, J. D. (1976). Sound production by the western rock lobster *Panulirus longipes* (Milne Edwards). *J. Exp. Mar. Biol. Ecol.* **23**, 191-209.

Moulton, J. (1957). Sound production in the spiny lobster *Panulirus argus* (Latreille). *Biol. Bull.* **113**, 286-295.

Moulton, J. (1958). Age changes in stridulation and the stridulatory apparatus of the spiny lobster, *Panulirus argus* (Latreille). *Anat. Rec.* **132**, 480.

Mulligan, B. E. and Fischer, R. B. (1977). Sounds and behavior of the spiny lobster *Panulirus argus*. *Crustaceana* **32**, 185-199.

Niederegger, S. and Gorb, S. (2006). Friction and adhesion in the tarsal and metatarsal scopulae of spiders. *J. Comp. Physiol. A* **192**, 1223-1232.

Parker, T. J. (1878). Note on the stridulation organ of *Panulirus vulgaris*. *Proc. Zool. Soc. Lond.* **1878**, 442-444.

Parker, T. J. (1883). On the structure of the head in *Palinurus* with special reference to the classification of the genus. *Nature* **29**, 189-190.

Patek, S. N. (2001). Spiny lobsters stick and slip to make sound. *Nature* **411**, 153-154.

Patek, S. (2002). Squeaking with a sliding joint: mechanics and motor control of sound production in palinurid lobsters. *J. Exp. Biol.* **205**, 2375-2385.

Patek, S. N. and Oakley, T. H. (2003). Comparative tests of evolutionary tradeoffs in a palinurid lobster acoustic system. *Evolution* **57**, 2082-2100.

Paterson, N. F. (1968). The anatomy of the cape rock lobster, *Jasus lalandii* (H. Milne Edwards). *Ann. S. Afr. Mus.* **51**, 1-232.

Persson, B. N. J. (2000). *Sliding Friction: Physical Principles and Applications*. Berlin: Springer-Verlag.

Phillips, B. F., Cobb, J. S. and George, R. W. (1980). General biology. In *The Biology and Management of Lobsters: Physiology and Behavior*. Vol. 1 (ed. J. S. Cobb and B. F. Phillips), pp. 1-82. New York: Academic Press.

Rabinowicz, E. (1995). *Friction and Wear of Materials*. New York: John Wiley and Sons.

Roberts, A. D. (1971). The shear of thin liquid films. *J. Phys. D Appl. Phys.* **4**, 433-441.

Roberts, A. D. and Tabor, D. (1971). The extrusion of liquids between highly elastic solids. *Proc. R. Soc. Lond. A Math. Phys. Sci.* **325**, 323-345.

Scherge, M. and Gorb, S. (2001). *Biological Micro- and Nanotribology*. Berlin: Springer-Verlag.

Schumacher, R. T., Garoff, S. and Woodhouse, J. (2005). Probing the physics of slip-stick friction using a bowed string. *J. Adhes.* **81**, 723-750.

Smale, M. (1974). The warning squeak of the Natal rock lobster. *S. Afr. Assoc. Mar. Biol. Res. Bull.* **11**, 17-19.

Urbakh, M., Klafter, J., Gourdon, D. and Israelachvili, J. (2004). The nonlinear nature of friction. *Nature* **430**, 525-528.

Woodhouse, J., Schumacher, R. T. and Garoff, S. (2000). Reconstruction of bowing point friction force in a bowed string. *J. Acoust. Soc. Am.* **108**, 357-368.

Yoshizawa, H. and Israelachvili, J. (1993). Fundamental mechanisms of interfacial friction. 2. Stick–slip friction of spherical and chain molecules. *J. Phys. Chem.* **97**, 11300-11313.